Astron. Astrophys. 297, 61–76 (1995)

ASTRONOMY
AND
ASTROPHYSICS

Detectability and incidence of E+A galaxies in the distant cluster Cl0939+472 (z=0.41)*

P. Belloni[1], **A.G. Bruzual**[2,3], **G.J. Thimm**[1], **and H.-J. Röser**[1]

[1] Max-Planck Institut fur Astronomie, Königstuhl 17, D-69117 Heidelberg, Germany
[2] Landessternwarte, Königstuhl, D-69117 Heidelberg, Germany
[3] CIDA, Apartado Postal 264, Merida 5101-A, Venezuela
email:belloni@mpia-hd.mpg.de

Received 3 June 1994 / Accepted 12 October 1994

Abstract. We present results of a study of E+A galaxies in the cluster Cl0939+472 (z=0.41). We have used a series of narrow-band filters (FWHM $\simeq$ 90–200 Å) covering the range from 3800 to 9200 Å, and broad band B, R, I filters to obtain low resolution spectra for all galaxies brighter than R=22.5 mag in a 5′ x 5′ cluster field. Two of the narrow-band filters have been chosen to measure the 4000 Å-break index, and 3 filters were centered on the H_β, H_γ and H_δ lines which are indicators of recent star formation. Template spectra were fitted to the low-resolution spectral energy distributions in order to determine the redshift and to assign a corresponding morphological type for each galaxy in the sample. The E+A templates were derived from a model which assumes that a strong star formation episode took place in an early-type galaxy 1–2 Gyr before its observational epoch (post starburst models).

We detected 35 E+A galaxies in this part of the cluster, 21% of the total number of galaxies investigated. Their projected radial distribution shows that they are less concentrated than ellipticals. Moreover, we identified half of them on high resolution HST images (Dressler 1992, 1993). Their morphology indicates that this kind of activity is associated with disk-like systems or mergers. Two cluster members, an unusually blue elliptical galaxy and a merger, seem to be going through an early phase of the starburst evolution, in which the second burst is still ongoing.

Key words: distant clusters – galaxies: evolution – galaxies: photometry

1. Introduction

The spectroscopic survey of high-redshift ($z \lesssim 0.5$) clusters of galaxies by Dressler & Gunn (1983, 1992), Couch & Sharples (1987) and others have confirmed the conclusions derived from the photometric data of Butcher & Oemler (1978): a significant evolution in the cluster galaxy population has occurred over the past $\sim$ 5 Gyr. These studies suggest that the situation is more complex than expected and that the Butcher-Oemler effect is more appropriately formulated in terms of the passive-to-active galaxy ratio rather than that of the blue-to-red ratio. The passively evolving galaxies are the ellipticals and S0 systems. Star formation in these ceased at least several Gyr ago, and they constitute 80-85% of the population in the core (inner several hundred Kpc) of nearby rich galaxy clusters (Butcher & Oemler 1978, 1984).

The studies of Dressler & Gunn (1992; hereafter DG92) have revealed that $\sim$ 30% of the galaxies in distant clusters are active. The class of active galaxies can be subdivided into those with and without emission lines. The spectra of emission-line galaxies range from those of spiral-like galaxies with ongoing star formation to starburst galaxies with large star formation rates and, exceptionally, to active galactic nuclei with high-excitation spectra. The other type of active galaxies in high-z clusters show weak or no emission lines but unusually strong Balmer absorption lines, colors ranging from those typical of an elliptical galaxy to 0.2–0.3 mag bluer, and metallic feature strengths typical of an underlying old stellar population. These objects have been called E+A because such a spectrum is well reproduced by an intense short-lived episode of star formation (resulting about 1 Gyr later in a significant population of A-stars) occurring in a galaxy with an old stellar population (E). E+A spectra are not typical of the low-redshift luminous galaxy population (Dressler & Gunn 1982, 1983, 1987).

If we accept the post starburst interpretation of the E+A phenomenon, we are faced with the obvious questions of what has caused the starbursts and why were they more prevalent in the past. Environmental effects can be at work. Evidence that galaxy mergers and interactions play a role in driving star formation has accumulated, despite the fact that the high velocity dispersion in clusters ($\geq$ 1000 km s^{-1}) is unfavorable to such encounters. Lavery & Henry (1988) and Lavery et al.

Send offprint requests to: P.Belloni

* Tables 7 and 8 are also available in electronic form at the CDS via anonymous ftp 130.79.128.5)

(1992) have obtained deep images of blue galaxies in several of the nearer Butcher-Oemler clusters (A963, A211, A2125) under good seeing conditions, and have shown that many of these galaxies are in fact multiple systems.

Another possible environmental effect is the compression of gas in gas-rich galaxies by ram pressure resulting from their motion through the intercluster medium (Dressler & Gunn 1983). Indeed, an alternative interpretation of the E+A spectral features is given by the spiral stripping model in which, instead of an additive burst of star formation, the removal of the gaseous disk of a spiral galaxy is required. A galaxy that forms stars continuously for several billion years and then stops will have an E+A spectrum 1–2 Gyr after star formation ends. Models of late-type galaxies with truncated star formation have been calculated by Dressler & Gunn (1983), Couch & Sharples (1987) and Newberry et al. (1990).

Galaxies might have experienced a starburst phase more frequently in the past, independent of the extreme environmental conditions that characterize galaxy clusters. Evolution is detected also in field galaxies (Broadhurst et al. 1988; Colless et al. 1990, 1993) but the relation between field and cluster evolution is at present not well understood. The redshift range $0.2 \leq z \leq 0.4$ seems to be particularly critical in this respect. Most of the faint blue objects responsible for the excess of counts at faint magnitudes, interpreted as either starbursts, dwarf galaxies or systems bound to merge, have this low redshift (Colless et al. 1993; Cowie et al. 1992a, 1992b). An essential contribution has come from HST observations of the morphology of galaxies in distant clusters (Dressler 1993; Couch et al. 1994; Dressler et al. 1994). However, morphology alone cannot clarify if these spectral peculiarities are produced by the unusual conditions existing in clusters at earlier epochs, or if they are related to the evolution of galaxies in general.

Since multifiber spectroscopy does not work efficiently at these low brightness levels, typically R=21–23 mag, the requirements of establishing a secure membership (instead of a statistical membership) and obtaining the spectra of a significant number of objects, remain the main observational obstacles in this field. Therefore, new observational approaches have been undertaken, in an attempt to overcome the problems of classical spectroscopy and photometry.

This paper is part of an extensive study of the galaxy population in medium to high redshift clusters. The first results of this project has been obtained by Thimm et al. (1994). They used a Fabry-Perot Interferometer (hereinafter FPI) to search for redshifted [OII]λ3727 and [OIII]λ5007 line emission from galaxies with ongoing star formation in the cluster Cl1409+524 (z = 0.46). They also showed that an appropriate combination of broad and narrow band filters can detect features typical of elliptical galaxies, determining thus their cluster membership. In this paper, we focus our attention on E+A galaxies. We have computed E+A templates adopting the post starburst picture using the isochrone synthesis models of Bruzual & Charlot (1993, hereafter BC93). These templates were used to systematically look for the frequency of the E+A phenomenon in this cluster. The study of the elliptical population was also undertaken in detail in order to have a reliable estimate of the significance of the E+A phenomenon in the context of the cluster population. A systematic analysis of the galaxies with ongoing star formation will be the necessary next observational step to quantify the whole activity in Cl0939+472.

Table 1. Log of cluster observations

filter [nm] (1)	date	t [sec] (2)	seeing ["]	feature
440/115	20.11.92	3100/5	$\leq$ 1.0	B
530/35	21.11.92	4000/4	1.2	
543/13	22.11.92	6000/4	1.0	$\tilde{D}^{-}_{4000}$
554/10	22-23.11.92	5500/4	1.0	
562/10	23-24.11.92	7150/5	1.2	
577/12	23-26.11.92	6000/4	1.0	$\tilde{D}^{+}_{4000}$
614/26	24.11.92	4500/3	1.2	
655/169	20.11.92	900/3	$\leq$ 1.0	R
656/17	26.11.92	7200/5	1.0	
683/9	25-26.11.92	7500/5	$\leq$ 1.0	H_β
726/16	25.11.92	6000/4	1.0	
820/130	20.11.92	600/2	$\leq$ 1.0	I

(1) mean wavelength of filter passband/FWHM of filter, (2) total exposure time/number of exposures

The observations and the reduction of the photometric and spectrophotometric data are described in Sect. 2. In Sect. 3 we describe the main characteristics of the E+A models used as templates. The approach used for the determination of the galaxy redshift and morphological type, and the results of our study are presented in Sect. 4. A discussion of the properties of the E+A galaxies in this cluster follows in Sect. 5.

2. Observations and data reduction

2.1. Filter setup

The observations described in this paper were obtained at the prime focus of the 3.5 m telescope on Calar Alto (Spain) in November 1992. All nights were photometric with an average seeing of 1". We used a 1024^2 Tektronix CCD (pixel size 25 μm and 8 e^- readout noise) with a scale of 0.53"/pix and a field of view of $7' \times 7'$. The log of our observations of Cl0939+472 (Abell 851) is shown in Table 1.

The effective transmission for each filter/detector combination is displayed in Fig. 1. The filters were selected to examine as accurately as possible the spectral energy distribution (SED) of ellipticals and E+A galaxies at the cluster redshift. Of the strong Balmer absorption lines characterizing the spectrum of E+A galaxies, the H_δ and H_γ lines are covered by the filters 5430/130 Å and 5770/120 Å (see Table 1) which also measure the amplitude of the 4000 Å-break, observed at λ=5640 Å in this cluster. The filter 6830/90 Å was placed on the redshifted H_β line (rest frame λ_c=4845 Å). This filter provides a good compromise between an accurate wavelength determination (a cluster velocity dispersion of 1000 km s^{-1} results in $\Delta\lambda$ = 16

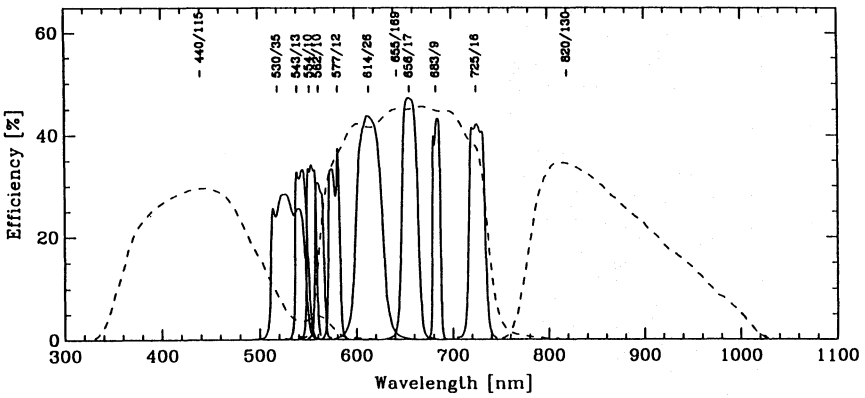

Fig. 1. Total efficiency of the filter+detector system used to sample the spectral energy distributions of the cluster galaxies

Å) and the faintness of the objects. Finally, the broad B, R, and I bands measure the galaxies' global spectral shape.

2.2. *Basic image reduction*

Our CCD frames were corrected for DC-offset averaged on the overscan area to take into account its time variation. No dark current was detected. For the basic image reduction we followed the procedures described in Röser & Meisenheimer (1991).

For every filter we obtained several exposures of the twilight sky. In this way we corrected for the fixed pattern noise and global sensitivity variations (multiplicative flat field component). When this procedure did not succeed in flattening the science frame's background to better than 1%, we used the science frames themselves to produce an additional multiplicative model of the background (MIDAS procedure FLATSKY). Only the I filter did show residual fringes caused by strong night sky emission. For this filter the science frames were used to derive a fringe frame (Röser & Meisenheimer 1991). This was treated as an additive flat field component, i.e. it was scaled according to the single frame background and then subtracted from the science frame after multiplicative flat field correction.

2.3. *Selection of a flux limited sample*

Given the extreme richness and large angular size of this cluster ($9' \times 9'$ according to Gunn & Oke 1975) only a limited region could be analyzed with our detector. Of the total available cluster field of $7' \times 7'$, our analysis was limited to a field of $5' \times 5'$, corresponding to an absolute dimension of 2.2×2.2 Mpc ($H_0 = 50$ km s^{-1} Mpc^{-1} and $q_0 = 0$ throughout this paper). We centered our field so as to cover not only the central part but also the SE outskirts of the cluster (up to a radius of about $4'$), allowing us to study the radial distribution of the cluster members.

The INVENTORY package implemented in MIDAS was used to extract from this field a statistically complete sample of objects. These are automatically classified as extended or stellar, and two magnitudes are assigned to each detected object, one inside a fixed circular aperture and one at a given isophotal level. However, we used this package only in its detection mode, leaving the task of object classification and photometry to a more accurate ad hoc procedure.

A deep R exposure of the cluster was taken as a reference frame for object detection. To assure completeness at a given magnitude level, INVENTORY must first be calibrated. For this purpose we observed the standard star HZ44 at an air mass negligibly different from that of the cluster. From the Massey et al. (1990) spectrum of HZ44 and the spectrum of α Lyrae, we derived the HZ44 magnitude in our R filter. We then fixed the INVENTORY photometric zero point, by running it on the HZ44 frame with a $10''$ photometric aperture and constraining the resulting magnitude to the predicted value. Our sample was finally defined by extracting all 780 objects brighter than R=23.5 mag above an isophotal level of 25.5 mag/$\square''$.

2.4. *Photometry*

Our cluster field is very crowded (Fig. 2). Rather than using a simple fixed aperture photometry to extract fluxes, we applied a weighted summation procedure, extensively described by Röser & Meisenheimer (1991). The width of the weighting function was chosed individually for each frame in such a way as to produce an effective resolution of all measurement of $1.8''$. FWHM. A window of $22'' \times 22''$ around the objects was used to determine the sky background.

High accuracy in the central coordinates of the objects is essential, so that for all the exposures the same region of the objects is sampled. Therefore the positions of reference stars were measured in all images and aligned with an accuracy of $0''.05$. We did not add frames taken with the same filter. Instead, for every frame galaxy's counts were independently measured and finally added according to their statistical weights. The filter data were flux calibrated using the count to flux conversion factor derived from the spectrophotometrically observed field star (see Sect. 2.5). The error of each photometric measurement was calculated from the photon statistics and a final uncertainty $\Delta m_B \simeq 0.15$, $\Delta m_R \simeq 0.07$, and $\Delta m_I \simeq 0.09$ was derived as the mean error values in the broad band filters for all objects brighter than R=22.5 mag. For a typical narrow band magnitude this error corresponds to $\Delta m \simeq 0.2 - 0.3$.

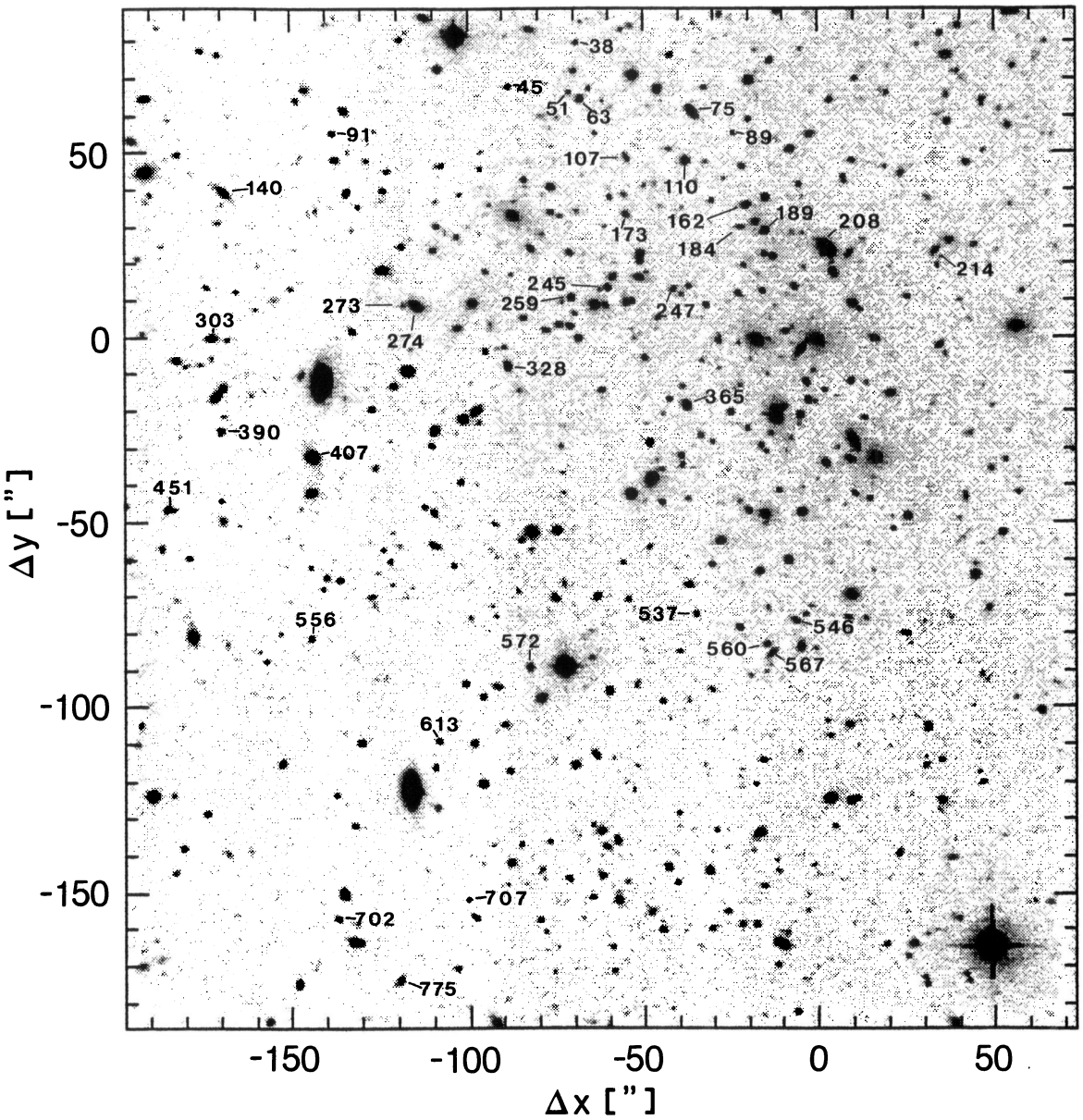

Fig. 2. Red image of our 5′x 5′ field in Cl0939+472. The positions of the E+A galaxies are shown. The zero value in the coordinates marks the cluster center. North is up, east to the left

2.5. Flux calibration

For the relative flux calibration of the filter data we used a spectrum of a star in the cluster field (α=09^h 39^m 54^s.0, δ=47°11′20″) (Fig. 3). The main advantage of this procedure is that the cluster calibration is then unaffected by variations of the photometric conditions during the night. In order to cover the wavelength range 3800−9200 Å required by our filters with sufficient resolution, we used a blue grism with a λ_c=5100 Å and a dispersion of 21.2 nm/mm, and a red one with λ_c=7700 Å and a dispersion of 29 nm/mm. Wavelength calibration was performed by means of a Hg-Cd comparison spectrum, providing a wavelength accuracy of ± 0.5 nm. The standard stars GD140 and HZ44 were used for flux calibration (Massey et al. 1990). The red and blue spectra were then rebinned to a final dispersion of 8 Å/pixel.

As a check, the flux calibration obtained from HZ44 as described in Sect. 2.3 was used to calibrate the spectrum of the standard star GD140. A significant deviation ($\simeq$ 10%) from the values reported in the literature was evident below 4200 Å. This was most likely due to the large uncertainty in the extinction correction in this wavelength range. We improved the calibration of the field star below 4200 Å by selecting from the Gunn & Stryker (1983) atlas the stellar spectrum that best matches its SED and absorption line strength. A G4V star turned out to be a good fit. The spectrum of the field star was finally replaced by that of a G4V star below λ = 4300 Å. No interstellar correction

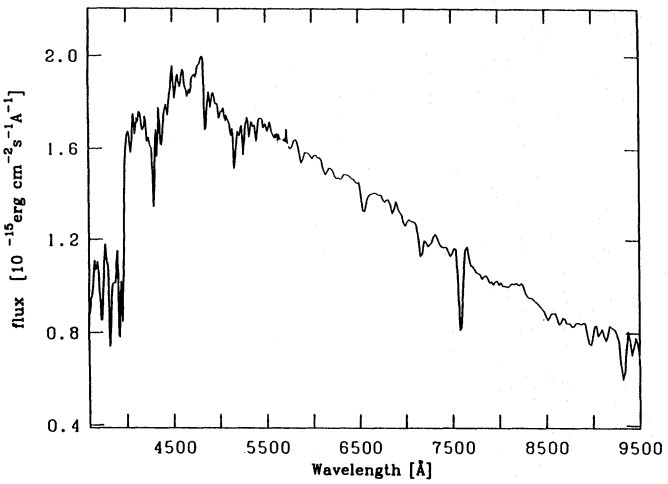

Fig. 3. Spectrum of the star in the field of Cl0939+472 used to calibrate the filter data. Its spectral type is G4V

was applied because in the direction of Cl0939+472, E(B–V) $\leq$ 0.03 (Burstein & Heiles 1982).

Combining this calibration spectrum with the filter/detector system efficiency curves, we obtained the count to flux conversion factors needed for the cluster data.

2.6. The $\tilde{D}_{4000}$ index

The 4000 Å-break is a prominent feature in the SED of elliptical galaxies which allows the redshift to be measured with an accuracy $\sigma_z \simeq 0.010$ (Thimm et al. 1994). The D_{4000} index amplitude is a valuable indicator for the presence of a passively evolving stellar population. It traces the main sequence stars near the turnoff and provides a fair estimate of the absolute age of a stellar population. We use D_{4000} as an indicator of the variations in the stellar content in a normal elliptical galaxy caused by a second burst of star formation of limited duration. Stars more massive than 2 $M_\odot$ expire about 1 Gyr after this burst, leaving no stars to supply ionizing radiation, and the longer-lived A-type stars dominate the spectral features. The contribution of the A-type stars increases the flux below 4000 Å and lowers D_{4000}. This index is thus a powerful tool for distinguishing a passively evolving normal elliptical from one in which a recent episode of star formation has taken place.

Since spectra are not available for our galaxy sample, the standard definition of the D_{4000} index is impractical. We introduce a similar photometric index using the filters 5430/130 Å and 5770/120 Å, with restframe wavelengths of 4100 and 3860 Å respectively, which reproduces the index defined by Bruzual (1983) as accurately as possible. For our galaxy sample the D_{4000} index is defined as

$$\tilde{D}_{4000} = 1.162 \times F_\lambda(5770/120)/F_\lambda(5430/130). \quad (1)$$

The factor 1.162 results from the transformation of our measured F_λ fluxes to F_ν units.

3. Modeling the spectral energy distribution of E+A galaxies

We have computed models to reproduce the SEDs of E+A galaxies based on the isochrone synthesis spectral evolution code of BC93. These models do not consider the chemical evolution of the stellar population and assume that at all epochs stars of only solar metallicity are formed with a constant initial mass function (IMF). Without loss of generality, the models discussed here were computed assuming that stars always form in the mass range from $m_l = 0.1\ M_\odot$ to $m_u = 125\ M_\odot$ following the Salpeter (1955) IMF. Neglecting chemical evolution is justified in our case because chemically evolving models predict no major changes in the shape of the SEDs at $z = 0.41$ with respect to the solar metallicity ones (Worthey 1992). In particular, the value of D_{4000} does not differ appreciably from the value for solar metallicity models for the range of metallicities observed in present-day galaxies (Charlot et al. 1993; González 1993). Extinction by dust should produce negligible effects in D_{4000} due to the narrow wavelength range involved. Large amounts of dust can redden the observed galaxy SEDs resulting in a tendency by our algorithm to assign an older template to these galaxies.

As in BC93, the evolving SED of elliptical galaxies is described by a model in which star formation takes place at a constant rate $\psi_1 = S_1\tau_1^{-1}$ during a burst phase lasting from $t = 0$ to $t = \tau_1$. To simulate the SEDs of E+A galaxies we assume that a second burst of star formation takes place in an elliptical galaxy at $t = \tau_B > \tau_1$. This second burst is characterized by a constant star formation rate $\psi_2 = S_2\tau_2^{-1}$ and lasts for a length of time τ_2. The star formation rate for the combined model is then given by

$$\psi(t) = \begin{cases} S_1\tau_1^{-1}, & \text{if } 0 \leq t \leq \tau_1; \\ S_2\tau_2^{-1}, & \text{if } \tau_B \leq t \leq \tau_B + \tau_2; \\ 0, & \text{otherwise.} \end{cases} \quad (2)$$

In these non-dynamical models, no restriction is placed on the mass ΔM_2 added to the mass M_1 of the original galaxy by the second burst. At any time $t > \tau_B$ we have

$$\frac{\Delta M_2(t \geq \tau_B)}{M_1} = \frac{S_2}{S_1}\frac{(t - \tau_B)}{\tau_2}, \quad (3)$$

where we have used that $\tau_B > \tau_1$ and $M_1 = \psi_1\tau_1 = S_1$. The maximum value of (3) is then

$$\frac{\Delta M_2(t \geq \tau_B + \tau_2)}{M_1} = \frac{S_2}{S_1} \quad (4)$$

In the rest of this section we summarize the properties of these models which are of interest for our study of Cl0939+47. A more general and detailed account of the E+A models will be presented elsewhere (Bruzual & Belloni 1994).

In Table 2 we list the values of the parameters used to build the two-burst models explored in this paper. Model 0 corresponds to the 1 Gyr burst model used by BC93 to reproduce the SED of normal elliptical galaxies (their Fig. 5) and is used here as a reference model. For all the models $S_1 = 1$. In Fig. 4 we show the evolution in time of B-R, R-I, B-I, and D_{4000} for the models listed in Table 2. These quantities are shown as differences with respect to model 0 in the Cl0939+47 observer

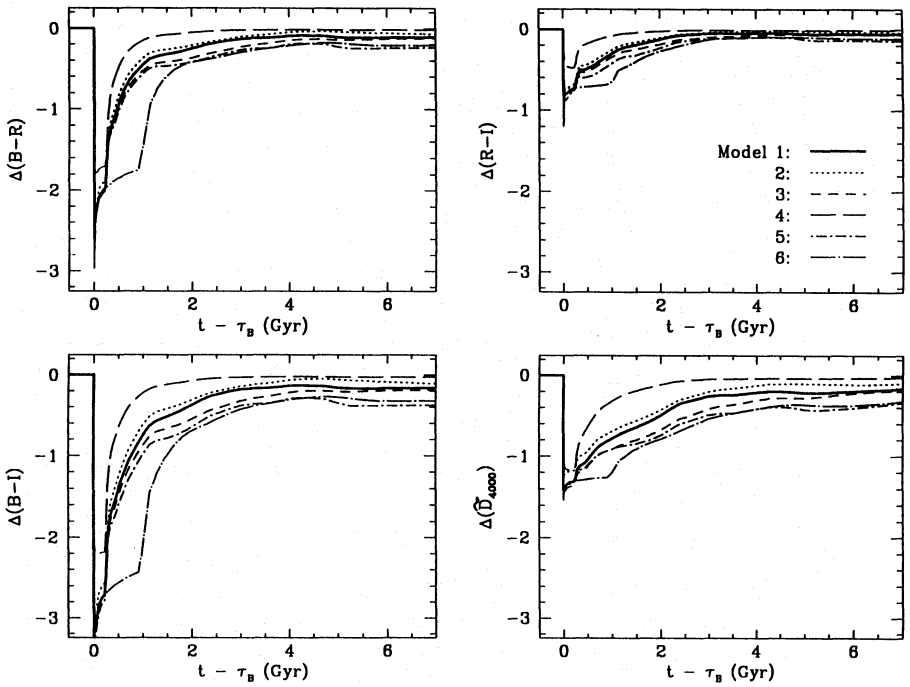

Fig. 4. Evolution in time of B−R, R−I, B−I, and $\tilde{D}_{4000}$ for the models listed in Table 2. These quantities are shown as differences with respect to model 0 in the Cl0939+472 observer frame. They were computed after redshifting the model SEDs to $z = 0.41$, and should not be used for different values of z. The lines for models 2 and 3 have been shifted horizontally in order to plot all of them in a common post-burst time scale

Table 2. E+A model parameters

Model	τ_1 [Gyr]	ψ_1 [$\frac{M_\odot}{Gyr}$]	τ_B [Gyr]	τ_2 [Gyr]	$\frac{\Delta M_2}{M_1}$
0	1	1			
1	1	1	9.5	0.25	0.250
2	1	1	7.0	0.25	0.250
3	1	1	12.0	0.25	0.250
4	1	1	9.5	0.25	0.025
5	1	1	9.5	0.25	2.500
6	1	1	9.5	1.00	1.000

Table 3. Properties of model 0

	Listed	B−R	R−I	B−I	$\tilde{D}_{4000}$
At 13.5 Gyr (BC93)		2.80	1.17	3.96	2.70
Slope (Gyr^{-1})		0.03	0.02	0.05	0.04
Change from z=0 to z=0.41		-0.17	-0.11	-0.28	-0.22

frame. They were computed after redshifting the model SEDs to $z = 0.41$, and should not be used for different values of z. D_{4000} was computed from Eq. (1). The lines for models 2 and 3 have been shifted horizontally in order to plot all of them in a common post-burst time scale. The color evolution of model 0 in our observer frame is given in Table 3. These quantities can be used together with Fig. 4 to compute the two-burst model colors at any age of interest.

The closeness of the lines representing models 1, 2, and 3 in Fig. 4 indicates that τ_2 is a more relevant parameter than τ_B. The colors are dominated by the decay of the second burst, independently of the precise value of τ_B. As expected, models 4 and 5 show that the intensity of the second burst (as measured by $S_2 = \Delta M_2/M_1$) is important in determining the decay rate of the young population. The effects of the second burst in model 4, which has one tenth the intensity of the burst in models 1, 2, and 3, decay faster than in these models. Above a certain burst intensity the younger population dominates the older stars and determines the model colors, which stop becoming bluer with increasing S_2 (model 5 remains close to model 1). The duration of the burst τ_B determines the length of time over which the model remains considerably bluer than the passively evolving model 0. The main sequence stars aroud the turnoff of the young population are responsible for maintaining the model colors bluer than model 0 after $\simeq$ 1 Gyr measured from τ_B. They are more noticeable in B-I or D_{4000} than in B-R or R-I.

Since model 1 shows an intermediate behavior in all colors examined, we selected 8 SEDs from this model to build our E+A template. They are listed in Table 4, together with their B-R and B-I colors, and $\tilde{D}_{4000}$ index in the observer frame. For completeness we list the same quantities for the Coleman et al. (1980) SEDs. The individual SEDs are plotted in Fig. 5. In Table 5 we list the fractional contribution of the burst population to the total light in different bands (in the rest frame) for our E+A template.

The selection of the E+A SEDs was guided by their ability to reproduce the UV continuum (our bluest filter samples a central rest frame wavelength of 3100 Å) and the Balmer absorption line strengths of the few known post starburst galaxies members. By integrating our E+A models over wavelength, we obtain a mean equivalent width of Hβ+Hγ+Hδ ranging from 11 Å (youngest) to 5-6 Å (oldest), in agreement with Dressler (1983) published values. Moreover, we measured EW(Hβ+Hγ+Hδ) in the E+As serendipitously discovered by Todd et al. (1993) in the Corona

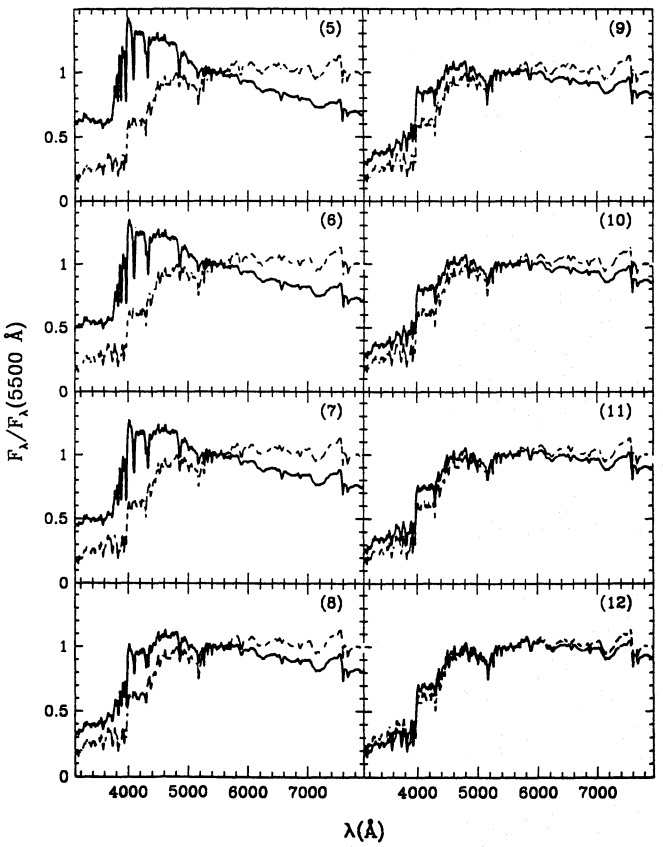

Fig. 5. SEDs from model 1 used to build our E+A templates. The number in each frame corresponds to the sequence number in Table 4. The dashed line plotted together with the E+As corresponds to model 0 at 13.5 Gyr (BC93)

Table 4. $\tilde{D}_{4000}$, B−R, B−I color indices for our template SEDs at z=0.41

No.	Hubble type	Gyr after s.b.	$\tilde{D}_{4000}$	B−R	B−I
1	Elliptical	–	2.49	2.64	3.85
2	Sbc	–	1.40	1.89	2.75
3	Scd	–	1.32	1.53	2.25
4	Im	–	1.19	1.08	1.58
5	E+A	0.50	1.57	1.90	2.51
6	"	0.64	1.61	1.97	2.63
7	"	0.75	1.67	2.08	2.78
8	"	1.14	1.83	2.33	3.18
9	"	1.61	1.96	2.41	3.33
10	"	1.90	2.04	2.45	3.41
11	"	2.30	2.19	2.51	3.53
12	"	3.00	2.35	2.61	3.68

Table 5. Fractional contribution of the burst component to the total light of an E+A galaxy for different wavelength bands of the Johnson standard system. Δt is the time in Gyr after the second burst

Δt	U	B	V	K
0.50	0.90	0.86	0.79	0.64
0.64	0.85	0.81	0.73	0.64
0.75	0.83	0.79	0.71	0.63
1.14	0.73	0.68	0.61	0.51
1.61	0.65	0.59	0.52	0.40
1.90	0.58	0.52	0.47	0.36
2.30	0.50	0.45	0.41	0.32
3.00	0.44	0.39	0.37	0.31

Borealis supercluster (kindly provided by the authors). After correcting them by 1/(1+z), we found values ranging from 9-5 Å, also in agreement with our models.

The SEDs listed in Table 4 define the templates that will be used in the rest of this paper to search systematically for the incidence of the E+A phenomenon in this cluster.

With the approach followed in this work, the ability to reveal signatures of the second burst phase essentially relies on the presence of A-stars, which all live for less than 3 Gyr. Thus, from our color synthesis algorithm, we found that galaxies with bursts more than 3 Gyr old cannot be distinguished from normal, passively evolving ellipticals. Older intermediate-age stars can be detected only by using spectral indices such as [Fe/H] that require high signal-to-noise spectra (Pickles 1985).

4. Results

4.1. Redshift and galaxy type

In order to establish cluster membership, i.e. galaxy redshift, and to assign a spectro-morphological class to the galaxies in our sample, the low-resolution SEDs were fitted with template spectra. This method was pioneered by Couch et al.(1983) and successively applied by Ellis et al. (1985), and Thimm et al. (1994).

Coleman et al. (1980) templates were used for the E, Scd and Irr galaxy types. For the Sbc spiral we preferred instead the BC93 spiral model characterized by an exponentially decreasing star formation rate with e-folding time τ = 7 and an age of 7.5 Gyr. In fact, when compared with the spectra in the Kennicutt (1992) atlas of nearby galaxies, we found that this model matches the observed spectrum of Sbc galaxies much better than the one in Coleman et al. (1980).

The template spectra were redshifted stepwise by Δz=0.002 to cover the redshift range between z=0.3 and z =0.75 and combined with the filter/detector response functions to predict the observed count rates at each z. For each galaxy, the redshift and the morphological type were obtained by a minimum χ^2 fit of the predicted to the observed count rates in the different filters. For those galaxies found to be ellipticals, we applied to the fluxes in our different filters bands a color-magnitude

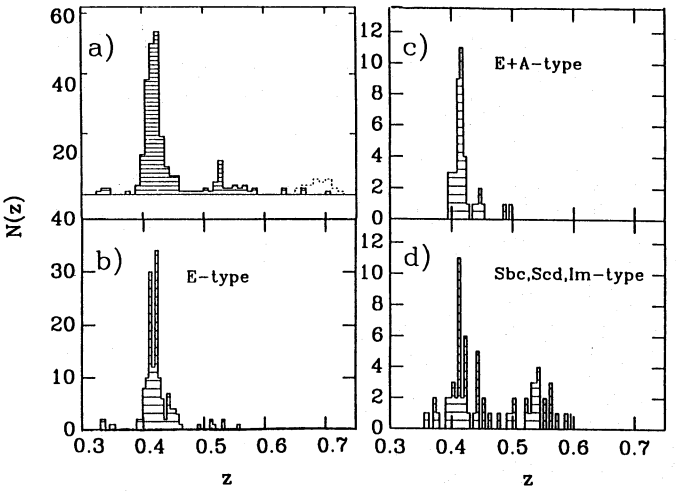

Fig. 6. a Redshift distribution for the 332 objects classified. The dotted line represents the contamination from M stars. **b**, **c**, **d** Redshift distribution respectively for E, E+A, Sbc, Scd, and Im galaxy types

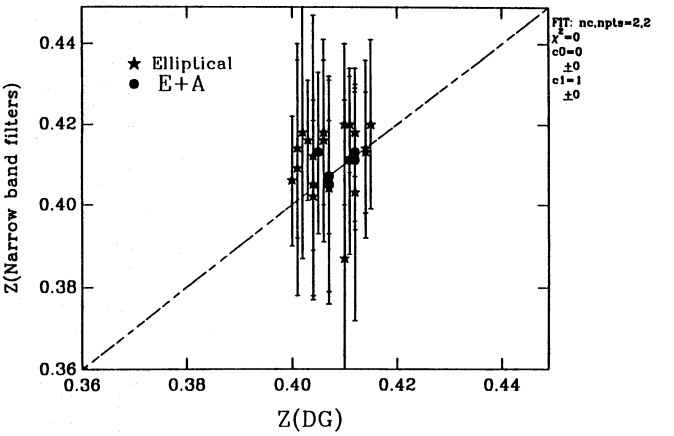

Fig. 7. Redshifts derived from our filter data compared with values obtained by Dressler & Gunn (1992). The dashed line represents the expected locus of the data points in the case of perfect agreement. The error bars indicate the 1σ-error of the redshift. The σ_z is 0.012

correction (CMC) according to Visvanathan & Sandage (1977). The CMC resulted in a mean B−R reddening of 0.2 mag and takes into account the fact that the SED in our template refers to the reddest ellipticals (see Thimm et al. 1994 for further details). The value for z obtained after applying the CMC was adopted for these galaxies.

The Coleman et al. (1980) spectra have low resolution (40 Å) in the optical range. To check how spectral resolution affects our results, we repeated the fitting procedure using some spectra for ellipticals by Kennicutt (1992), which have a resolution of 15 Å. The resulting differences were negligible.

Our original sample consisted of 780 objects. However, to improve the reliability of our results, this analysis has been restricted to objects brighter than R=22.5 mag, i.e. one magnitude brighter than INVENTORY limit (Sect. 2.3), i.e. 323 in total.

4.2. Redshift distribution

In Table 6 we present the results of the analysis for the Cl0939+472 field. Out of the 323 objects, 275 could be classified. This represents a success rate of 85% in the determination of redshift and corresponding morphological type derived from SEDs. In Table 7 we list the classified member galaxies brighter than R=22.5 mag according to their SEDs. The assignment of a morphological type to a galaxy on the basis of its SED is a priori a risky assumption. In fact the link between galaxy morphology and physical properties (the Hubble classification) might not be valid in the universe 5 Gyr ago . Anyway, the results presented in Sect. 5.3 make us confident of the reliability of this assumption. Table 7 shows that E-, E+A-, and S+Im-types are characterized by significantly different colors and values of the $\tilde{D}_{4000}$ break. The improvement achieved in the statistics over the most complete study to date of Cl0939+472 (DG92) is also evident. In particular, we note that the $\tilde{D}_{4000}$ index can be measured for more than one hundred galaxies, for which cluster membership is well established.

Table 6. Statistics of our analysis of the Cl0939+472 field for objects with $m_R \leq 22.5$

Total	Members	Backg.	Foregr.	Stars	Unclass.	Succ.
323	174	71	5	25	48	85%

Figure 6a shows the resulting redshift distribution for all objects classified whereas in Fig. 6b, 6c, and 6d they are discriminated by galaxy type. The prominent peak around $z = 0.41$ is due to the cluster. A marginal contribution from foreground objects is present. The bump visible at $z = 0.55$ is mainly due to field spiral galaxies. Contamination by M stars around $z = 0.7$ is shown with a dashed line (see below).

Figure 7 shows the accuracy achieved in the determination of the redshift for the elliptical and E+A population. The redshifts for 20 elliptical and 6 E+A spectroscopically confirmed members (DG92) are compared with our results. The standard deviation σ_z(narrowband − spectroscopic) = 0.015. From Fig. 7 is clear that our redshift values deviate systematically from the DG92 ones. After correcting for this offset σ_z drops to 0.010.

The spiral population lacks prominent features detectable with our filter setup. Therefore the membership determination for spirals has not been considered as reliable as that for ellipticals. A FPI is required to properly accomplish this task. However, for spiral galaxies a rough estimates of σ_z can be obtained from the shape and width of their redshift distribution around the mean cluster redshift (Fig. 6d). This gives a $\sigma_z \simeq 0.04$. Because this value is dominated by measurements errors, it is not an indication of the cluster velocity dispersion.

We assume that all elliptical and E+A galaxies in the range $0.385 < z < 0.430$ and all S/Im in the range $0.37 < z < 0.450$ are cluster members. Considering all the cluster galaxies, we obtain a mean redshift $z = 0.410 \pm 0.010$, in agreement with the DG92 value of $z = 0.407$. Although the accuracy in redshift

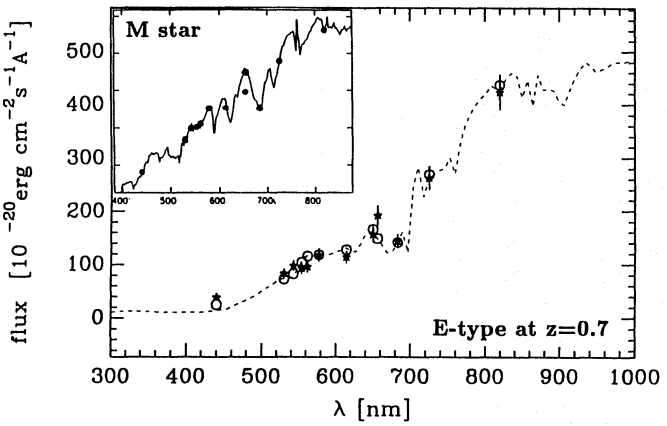

Fig. 8. SED of a MV star (from Gunn & Stryker 1983) convolved with our filter setup (upper left). The main panel shows how the points resulting from this convolution can be very well fitted with an elliptical galaxy at z≃0.75. The similarity of the two SED is striking

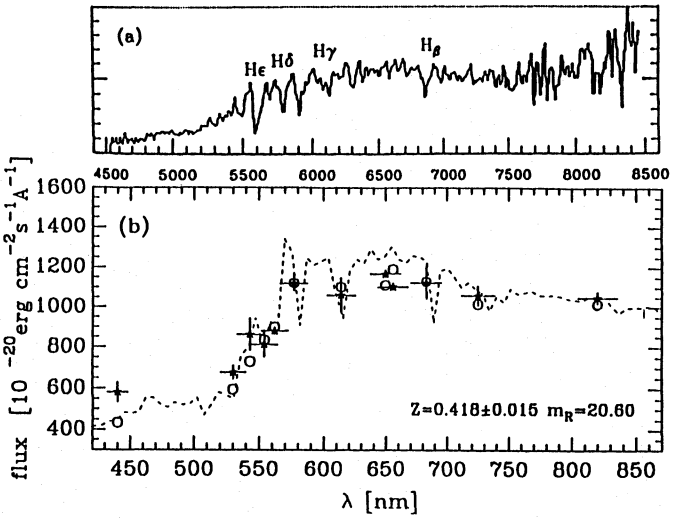

Fig. 9. a Spectrum of an E+A member in Cl0939+472 taken by Dressler & Gunn (1992). **b** Our reconstructed spectrum using multifilter photometry. The open circles represent the values expected by convolving the theoretical E+A spectral distribution (dashed) with the filters used; the filled ones are the observed data. The error bars show the 1σ-error of the photometry

achieved for the ellipticals is high, it is still not good enough to study the internal kinematics of distant cluster ellipticals.

4.3. Contamination from field galaxies and galactic stars

4.3.1. Contamination from field galaxies

Contamination by foreground galaxies is a well known problem since the work of Butcher & Oemler (1978). The standard photometric approach to account for it is to study a control field with the same observational setup used for the target cluster, and then derive from the control field the contribution of the field galaxy population. Thanks to our capability to identify the cluster members, we do not need to apply this procedure. The field contamination can be estimated directly in our cluster field. Outside the redshift window used to identify the cluster members, we found a total of 71 foreground and background objects. This is consistent with Tyson (1988) galaxy counts, which predict 75 field galaxies with R $\leq$ 22.50 in a 5′x 5′ field.

4.3.2. Contamination from galactic stars

Due to their high brightness level, 7 objects were immediately recognized as galactic stars. But the profiles of typical cluster galaxies have FWHM similar to those of the faintest stars, even with a 1″ seeing. So, distinguishing a galaxy at these redshifts from faint stars, is not a straightforward task. A first look at the redshift distribution showed a significant peak at z=0.7−0.8, mainly due to galaxies classified as ellipticals. Their red colors suggested contamination from galactic late-type stars. Therefore, to perform a more detailed analysis we computed synthetic fluxes for the SEDs of dwarf and giant M-type stars (Gunn & Stryker 1983) seen through our filter/detector system. These data points were then considered as an unknown input to our classification program.

Surprisingly, all these stars were systematically fitted with elliptical galaxies in the z =0.7−0.8 range because of the impressive similarity of these two types of SEDs (Fig. 8). This point should be carefully taken into account when extending this kind of photometric approach to high redshift (z=0.7−0.9) galaxy clusters. Broad band colors cannot distinguish between cool galactic stars and early type galaxies at $z \simeq$ 0.7-0.8; only a good choice of narrow band filters can do so.

Aware of the relevance of star contamination, we worried about the possible misidentification of K stars whose colors are closer to the E+A and spiral cluster members. Repeating the same procedure that we applied to the M stars to a subset of the K stars in the Gunn & Stryker atlas, we obtained reassuring results. A K-type star SED seen through our filters cannot be misidentified with an E+A member; eventually with a spiral at lower redshift ($z \simeq$ 0.3) but this does not constitute a problem for our cluster analysis.

In total we classified 20 objects as late-type stars. Comparing these results with the extrapolated (Bahcall & Soneira 1981a,b) counts for objects brighter than R = 22.50 mag in this area of the sky (Bahcall & Soneira 1981a,b), the agreement is excellent (27 predicted against 25 detected).

5. Characteristics of the E+A population

5.1. The post-starburst population

The main goal of this paper is to identify E+A cluster members. Figure 9 demonstrates how an E+A galaxy is successfully identified as a member by fitting a model template that reproduces the strong Balmer absorption lines and the shape of the continuum. The galaxy in the lower panel is classified as a post-starburst, seen 0.75 Gyr after the beginning of the second burst (model 7 in Table 4). By applying this procedure to our field, 35

Table 7. Discrimination among morphological types for Cl0939+472 members for objects with $m_R \leq 22.5$

Spectral type	DG92	This work	<B−R>	<B−I>	$<\tilde{D}_{4000}>$
Elliptical	22	110	2.40±0.17	3.55±0.26	2.21±0.35
E+A	6	31	2.03±0.17	3.01±0.32	1.81±0.23
Spiral & Im	2	24	1.37±0.34	2.11±0.34	1.30±0.22

member galaxies turned out to have an E+A spectrum. All six already known E+A members (DG92) were correctly classified and 29 new ones found. Table 8 lists the B−R, B−I and $\tilde{D}_{4000}$ values for all the galaxies classified as members and assigned an E+A spectral type.

Even though the number of cluster members classified as E+A appears large, they represent $21 \pm 7\%$ of the galaxy population studied. This fraction is in agreement with DG92 (6 E+As out of 30 members). The error was calculated using Poisson statistics.

We show in Fig. 10 the resulting fits for 15 E+A members arranged with increasing age after the second burst phase, together with five examples of the elliptical type. Note in the E+As the progressive decrease of the H absorption line strengths and of the blue flux, as well as the bluer continuum than in an elliptical galaxy below $\lambda \simeq 6000$ Å.

In our description of the E+A phenomenology by means of SED templates, we assume that the second burst of star formation is characterized by parameters valid everywhere in the cluster. The differences observed among the E+A SEDs are attributed to the spread in age after the burst. Alternatively, bursts of different strength and/or duration taking place simultaneously in the cluster, will result in post starburst galaxies with SEDs similar to those in our template, but with the same age after the second burst.

In an attempt to understand the burst history in the cluster, with these assumptions we looked at the spread in post-burst age of our 35 E+A members. The histogram in Fig. 11 shows the results, namely a roughly Gaussian distribution with a peak at the 1.60 Gyr old E+As. Actually, only a couple of E+A galaxies are detected during the early phases of the post starburst sequence.

In Fig. 12 we present $\tilde{D}_{4000}$ vs color index diagrams for the galaxy population in Cl0939+472. Typical errors in the photometry (see Sect. 2.5) are Δ(B−R)=0.15, Δ(B−I)=0.20, Δ(R−I)=0.10, and $\Delta(\tilde{D}_{4000}) = 0.07$. The amount of color evolution present at this redshift (Table 3) is comparable to these errors (see also Lilly 1987; Buzzoni 1989). Therefore, even if the procedure applied to establish membership and morphological type implicitly neglected evolutionary effects, we have confidence that our non evolved templates can reproduce the SEDs of the cluster members.

At first glance, Fig. 12 could suggest that broad band colors, coupled with the $\tilde{D}_{4000}$ index, are good star formation indicators so that no further information is needed to determine the spectro-morphological type of cluster galaxies. The following analysis will show that some caution is necessary. Elliptical galaxies form a relatively tight group which suggests that this population is homogeneous at $z \sim 0.41$. No CMC has been applied to the colors plotted in these figures and this can account for some of the scatter, for the discrepancy between the B−R and B−I colors in Table 4, and the observed ones in Table7. Compared to the ellipticals, E+A galaxies have bluer colors and lower $\tilde{D}_{4000}$ and the separation in these diagrams between early-type and E+A galaxies is fairly large (mean color and $\tilde{D}_{4000}$ values for the two classes are very different). However, the transition between these is almost continuous and some E+A galaxies overlap with the bluest (metal-poor) ellipticals. E+A galaxies are clearly separated from the spiral population too, because of their redder colors and higher $\tilde{D}_{4000}$. However, from colors alone the misidentification of early spirals in the cluster as E+As is still possible.

A further complication is caused by contamination from field galaxies. To illustrate how significant field contamination can be, we display in Fig. 13 the same diagram as in Fig. 12a, but for all the objects in our field brighter than R=22.5 mag. The positions occupied in this diagram by non-evolving E and Scd galaxies with redshift from 0 to 1 are also shown. Note the large extension of the region which overlaps with the cluster members (Fig. 12a). The information contained in the $\tilde{D}_{4000}$ and color indices is not enough to separate the field and cluster populations.

From the previous arguments one concludes that sampling the galaxy SEDs through several narrow band filters is necessary to successfully establish galaxy cluster membership and morphological type. Even though the 12 filters used in our analysis may appear excessive, our experience shows that if this number is drastically reduced, then (a) the accuracy in redshift required to establish cluster membership will not be achieved, and (b) the resulting low resolution SEDs will not be sensitive enough to the strength of absorption features to allow the kind of spectro-morphological classification that we have performed. Table 1 shows that our observations, including calibration spectra of field stars, were carried out in about 14 hours of telescope time. This seems reasonable for the amount of information obtained.

Compared with early-type members, the E+As do not seem to have a peculiar luminosity distribution in the cluster (Fig. 14). As discussed below, no correlation between the age of the burst and the galaxy projected spatial distribution was found.

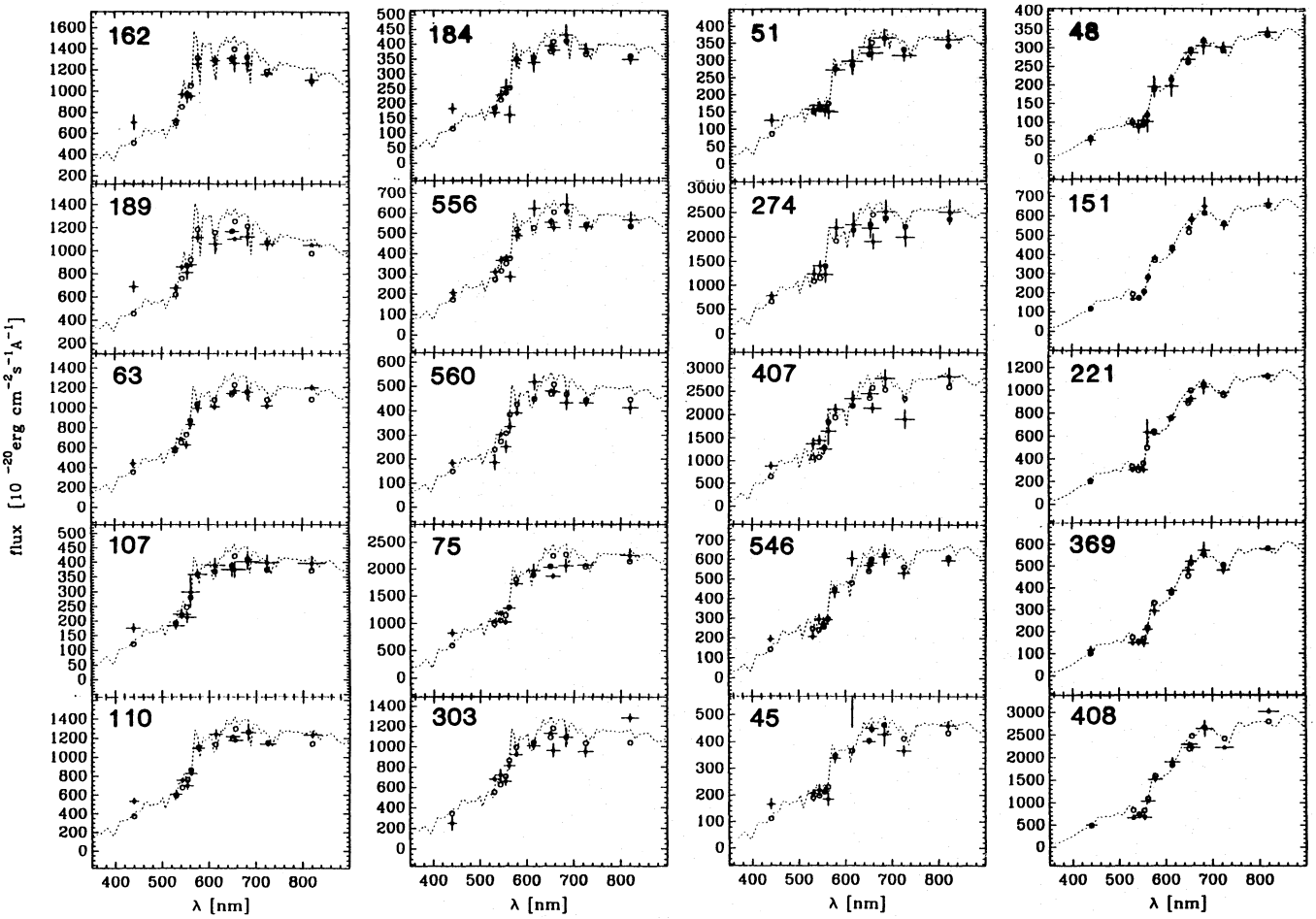

Fig. 10. Low resolution spectra for 15 objects classified as E+A galaxies in Cl0939+472 (same symbols as in Fig. 9). They are ordered according to their increasing age after the second burst. The galaxies 110, 162, 189, and 546 are already known to be members from Dressler & Gunn (1992). The last column shows spectral energy distributions of 5 elliptical members for comparison

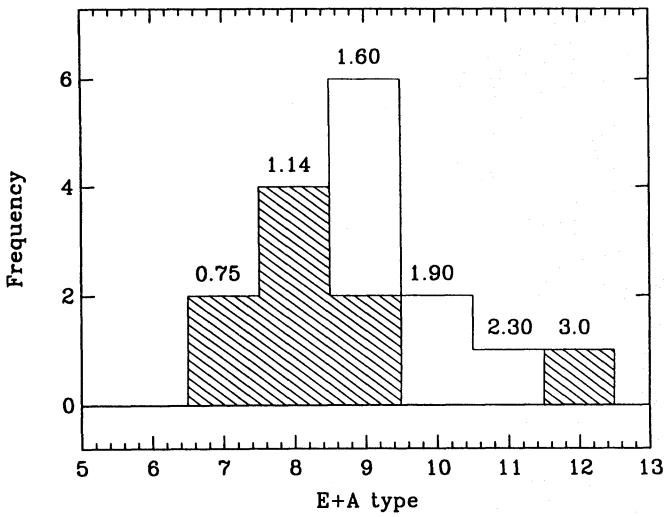

Fig. 11. Histogram of the age distribution of the 35 E+A members. The hatched region represents mergers and irregular galaxies, the blank one normal spirals (according to Dressler 1992). E+A types from 6 to 10 describe galaxies seen 0.75, 1.14, 1.60, 1.90 and 2.30 Gyr after the beginning of the second burst

Despite the good agreement between our field galaxy counts and the number expected from Tyson (1988) counts, we are still faced with the question of the nature of the 48 unclassified objects (15%). Most of these objects are likely to be field galaxies or spiral members, since they have colors systematically bluer than an elliptical or E+A cluster member. Also, our filter setup was optimized for the detection of elliptical and E+A galaxies at $z = 0.41$. Because the spirals in this cluster, as well as field galaxies with $0.3<z<0.75$, lack prominent features detectable with this setup, they are more difficult to classify. Finally, but very importantly, we are neglecting all objects outside the previous defined redshift window.

5.2. Radial distribution

Our determination of cluster membership allows us to analyze the radial distribution of the member galaxies without applying any correction for field galaxy contamination. Figure 2 shows how the early-type and E+A populations are distributed in projection.

Table 8. E+A galaxies in Cl0939+472. (1)-(2) Coordinates in arcseconds relative to the galaxy 259 in DG92, (3) redshift from DG92, (4) redshift derived in this work and (5) its 1-σ error, (6) Galaxy age after the beginning of the second starburst

No.	x (1)	y (2)	R	B-R	B-I	$\tilde{D}_{4000}$	z_D (3)	z (4)	σ_z (5)	Age (6)	Morph. HST
38	-73.29	79.70	22.19	1.47	2.40	1.46		0.418	0.040	1.90	
45	-92.55	74.98	21.83	1.99	3.05	1.81		0.420	0.022	1.90	
51	-74.66	73.17	22.02	2.12	3.14	1.02		0.428	0.040	1.90	
63	-71.35	71.43	20.70	2.06	3.04	1.70		0.412	0.018	1.14	
75	-37.13	67.60	20.07	2.03	3.07	1.71		0.418	0.024	1.60	
89	-24.80	61.21	22.12	1.98	2.91	1.71		0.420	0.0430	1.14	
91	-144.84	61.32	20.83	2.19	3.30	1.86		0.410	0.016	1.90	
107	-56.91	53.76	21.91	1.86	2.85	1.87		0.416	0.036	1.14	
110	-39.34	53.21	20.63	1.92	2.87	1.69	0.407	0.416	0.024	1.14	
140	-177.40	43.92	20.64	2.16	3.08	1.92		0.412	0.015	1.90	
162	-21.00	39.99	20.55	1.63	2.38	1.50	0.412	0.418	0.017	0.75	Im
173	-57.31	37.25	21.73	1.67	2.73	1.60		0.414	0.047	1.60	Sb
184	-22.64	33.42	21.85	1.87	2.67	1.76		0.420	0.023	1.14	Im
189	-15.35	32.34	20.67	1.61	2.42	1.51	0.412	0.420	0.020	0.75	Merger
208	3.25	27.13	19.73	1.92	3.04	1.80	0.407	0.4141	0.014	1.60	Merger
214	35.46	26.45	21.41	2.33	3.52	1.72		0.406	0.029	2.30	
247	-43.15	14.95	21.55	2.12	3.10	1.78		0.404	0.022	1.60	Im
273	-120.20	10.15	19.44	2.26	3.33	1.77		0.418	0.011	1.90	Sa
274	-124.10	10.07	22.49	2.13	3.22	1.81		0.396	0.029	1.90	
303	-180.97	0.58	20.71	1.83	2.90	1.49		0.410	0.023	1.14	
328	-92.97	-7.74	20.15	2.117	3.19	1.70		0.418	0.016	1.60	Sb
365	-39.14	-19.58	20.47	1.87	2.80	1.64	0.411	0.418	0.021	1.14	Merger
390	-178.24	-27.03	21.22	2.29	3.32	1.87		0.408	0.030	2.30	
407	-150.98	-34.45	19.86	2.14	3.22	1.71		0.398	0.030	2.30	
451	-194.04	-50.11	21.24	1.98	3.04	1.71		0.410	0.036	1.60	Sb
537	-36.29	-81.34	22.19	1.45	2.44	1.58		0.4141	0.035	1.14	Im
546	-6.39	-83.08	21.45	2.20	3.18	1.71	0.405	0.418	0.019	2.30	Im
556	-151.44	-88.30	21.49	2.11	3.06	1.55		0.420	0.022	1.14	
560	-14.87	-90.32	21.64	2.08	2.84	1.52		0.408	0.021	1.14	
567	-13.40	-92.93	21.34	2.18	3.14	1.66		0.410	0.025	1.60	Sc
572	-86.58	-97.01	21.09	2.01	3.14	1.48		0.418	0.034	1.90	Sb
613	-113.73	-118.75	21.80	1.56	2.48	1.86		0.414	0.042	1.60	
703	-141.68	-163.70	20.36	2.32	3.30	1.65		0.418	0.017	1.90	
707	-105.12	-165.38	22.28	2.48	3.54	1.64		0.414	0.028	2.30	
775	-125.29	-189.64	21.58	2.28	3.23	1.67		0.410	0.022	1.14	Sa

To obtain quantitative information, we binned elliptical and E+A galaxies in annuli about the central dominant galaxy (as in DG92). Because our cluster field is not symmetric with respect to this object, we applied to the galaxy counts a geometrical correction in the outer regions. Up to 90″ from the cluster center, the galaxies are sampled with a 20″ step size. Further out the sampling interval is 30″. In Fig. 15 a King profile, appropriate for a relaxed system, is fitted to the elliptical galaxy counts. It is characterized by a core radius r_c=50″, corresponding to 0.35 Mpc and a galaxy central density σ_o = 29 galaxies arcmin^{-2}.

The radial distribution of E+A galaxies is clearly different from that of the ellipticals. No central concentration is evident and the galaxies are spread all over the field. If anything, an overdensity is visible in an outer region at a radius of about 80″ (0.65 Mpc) from the center (Fig. 2).

The radial distribution of E+As shows no correlation with the age elapsed since the second burst. Such a correlation is expected in the gas stripping picture in which star formation is induced in an infalling gas-rich galaxy by ram pressure resulting from its first passage through the intercluster medium, producing a strong radial gradient in the colors and spectral properties of the blue galaxies (Evrard 1991). In such a scenario the starburst galaxies would preferentially be expected in a ring of radius close to 1 Mpc around the cluster center (the spherical shock site), and the increasingly red post-starburst galaxies should lie towards the center. The lack of such correlation could be a point in favor of a scenario in which no radial segregation by colors is expected, i.e. a merger scenario (see below).

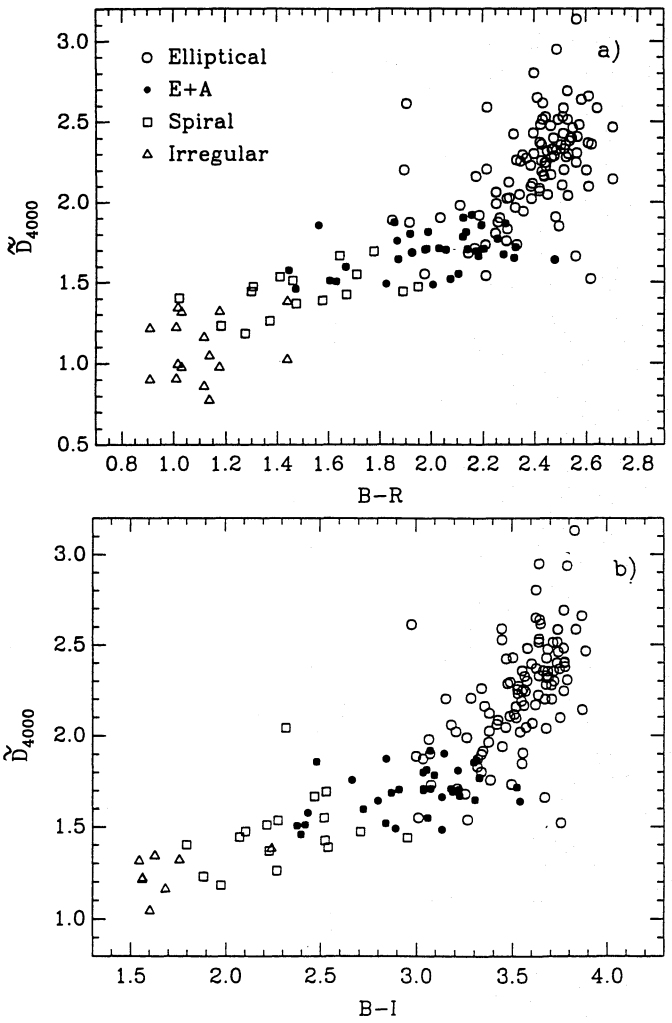

Fig. 12. a Diagram showing the $\tilde{D}_{4000}$ as a function of the B−R color for the Cl0939+472 members. No color magnitude correction has been applied to the fluxes of the elliptical galaxies. **b** Same as in **a** but for $\tilde{D}_{4000}$ as a function of the B−I color

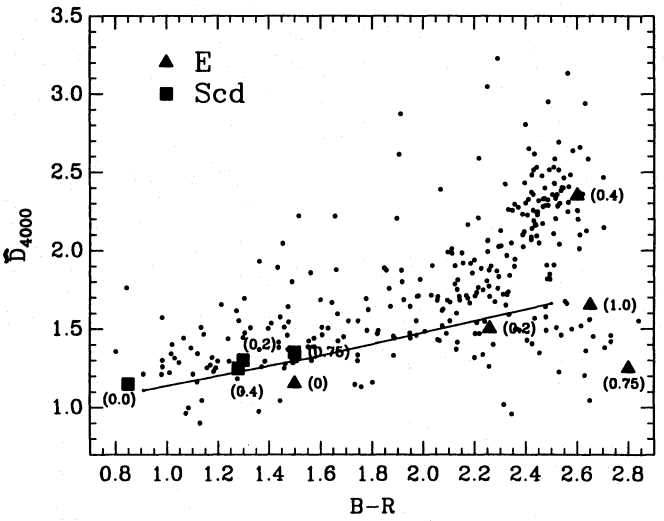

Fig. 13. Same as in Fig. 12a but displaying all objects classified with $m_R \leq 22.5$ in the cluster field. The thick line represents the upper limit of contamination by galactic stars. An elliptical and a spiral galaxy at z=0,0.2,0.4,0.75,1.0 are also showed to point out how critical the contamination from field galaxies can be

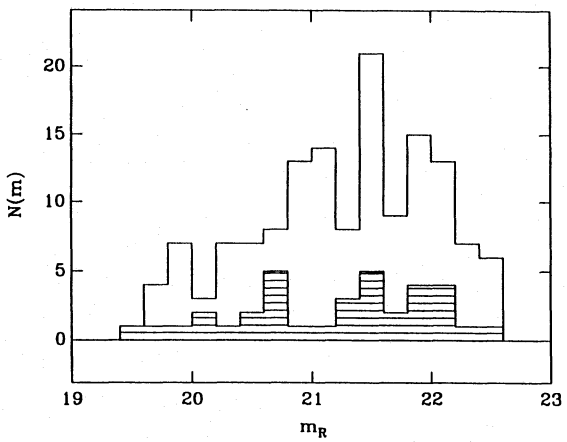

Fig. 14. Distribution of R magnitude for all E (open histogram) and E+A members (hatched histogram)

5.3. Morphology information

High spatial resolution images of distant clusters of galaxies are helpful in shedding some light on the evolutionary link between the dominant red population of the nearby clusters and their blue progenitors. We combined the HST morphological information available for two $1' \times 1'$ fields centered in the cluster (Dressler 1992) with our redshift and SED identification. Using the color-morphology diagram in Dressler (1993) and the DG92 photometry, we identified and obtained the morphological classification for 83 galaxies in our sample. Only 15 E+As were identified in the HST images. In Table 8 we indicate the HST morphological classification of E+A galaxies, when available. They turn out to be either mergers or disk-systems (the majority of them).

Observational evidence is increasing in this direction. HST images of the blue members in Abell 370 and AC114, characterized by active or recently completed star formation, show mainly disk-dominated systems (Couch et al. 1994). These cases could probably be better understood in the gas stripping picture in which a gas-rich galaxy is the site of the star formation activity. Mergers/interactions and ram-pressure stripping of galaxies are both plausible explanations of the appearance of E+A galaxies in high redshift galaxy clusters. However, this difference in physical processes does not affect our results, based on E+A post starburst templates. Indeed, Newberry et al. (1990) showed that the differences between the spectra obtained in the spiral stripped and post starburst models are not significantly large when compared to the resolution of the available data. Therefore, only details will change in this alternative scenario (for instance the interpretation of differences in the E+A SEDs in terms of time elapsed since the second burst) but not the basic results.

Table 9. Redshifts and morphological type for all objects that could be identified in Dressler (1992). Morphology derived with our SEDs is compared with that from HST. Same symbols as in Table 8

No.	Z_D	z	σ_z	Morph. type	Morph. HST	No.	Z_D	z	σ_z	Morph. type	Morph. HST
172		0.424	0.040	E	S0	317		0.516	0.046	E	S0
176	0.406	0.424	0.019	E	E	326		0.414	0.028	E	Sa
180		0.428	0.023	E	E	332		0.414	0.034	S	Sb
183		0.422	0.031	E	E	339		0.420	0.034	E	Sb
209	0.414	0.414	0.018	E	S0	340	0.406	0.412	0.027	Im	Merger
215		0.418	0.042	S	Sd/Im	345		0.412	0.012	S	S0
216	0.407	0.412	0.027	E	E	351		0.478	0.027	S	Sd/Im
217		0.424	0.020	E	E	358		0.420	0.024	E	Sb
218		0.406	0.020	E	S0	367		0.412	0.014	E	S0
221		0.412	0.015	E	E	369		0.420	0.022	E	Sa
234	0.406	0.422	0.035	E	E	370		0.412	0.010	E	S0
235		0.420	0.031	E	Sb	371		0.564	0.013	Im	Sc
240		0.442	0.027	S	Sb	374		0.530	0.049	S	Sd/Im
241		0.414	0.021	E	S0	378	0.415	0.422	0.022	E	Sa
243		0.422	0.030	E	S0	387		0.428	0.020	E	S0
245		0.414	0.024	Burst	E	398		0.540	0.035	S	Sa
251		0.420	0.029	E	E	399		0.464	0.016	Im	Sd/Im
259		0.448	0.019	Burst	Merger	410		0.420	0.027	E	S0
263	0.407	0.404	0.028	E	Sb	413	0.410	0.420	0.020	E	S0
265		0.428	0.037	E	Sa	449		0.532	0.034	E	S0
267		0.446	0.035	E	E	452	0.350	0.410	0.015	E	Sa
272	0.401	0.418	0.032	E	E	453		0.536	0.023	S	Sd/Im
279		0.420	0.021	E	S0	457		0.487	0.044	E+A	S0
282		0.438	0.033	E+A	S0	495	0.408	0.422	0.010	Ir	Merger
283		0.434	0.034	E	Sa	500		0.420	0.019	Im	Sd/Im
286		0.420	0.029	E	S0	505		0.726	0.021	E	E
288		0.452	0.036	E	Sa	523		0.412	0.015	E	Sa
290		0.422	0.024	E	Sa	542		0.394	0.030	E	Sc
292		0.420	0.026	E	Sb	543		0.444	0.030	E	Sb
293		0.420	0.024	S	Sb	548		0.408	0.017	E	Sa
299	0.404	0.412	0.035	E	E	561	0.414	0.422	0.015	E	Sa
302		0.412	0.023	S	Sb	586		0.412	0.015	S	Sa
304	0.411	0.420	0.023	E	E	593		0.458	0.032	E	E
314		0.420	0.014	E	S0	624		0.456	0.061	E	S0

The remaining 68 galaxies in our sample with HST morphology are listed in Table 9. We find that for 88% of these galaxies our classification based on spectroscopic properties matches Dressler HST morphological classification.

The spectral resolution attained with our filters is clearly unable to distinguish an elliptical SED from that of an Sa galaxy. Indeed the latter should show only a smaller $\tilde{D}_{4000}$ and [OII]λ3727 Å in emission (not detectable with our filters). We are aware that our accuracy in classifying SEDs of spiral galaxies is insufficient to resolve the different Hubble types. The irregular type should, however, be recognizable. In view of this, it is remarkable that only 9 galaxies in our sample show a serious discrepancy with Dressler classification.

A notable case is our galaxy #245, whose SED is plotted in Fig. 16, classified as an elliptical by Dressler (1993), but with g−r colors unusually blue (DG92). Our analysis confirms its peculiar blue color and establishes its membership. We initially classified this galaxy as irregular, but irregular and elliptical SEDs were so radically different that an explanation had to be found other than insufficient spectral resolution. It is well known that a burst of star formation involving only a few percent of the galaxy's gaseous content can radically change the galaxy colors, as long as it is ongoing and the underlying population is old. For our cluster analysis we selected post starburst models in which the burst is seen in its fading phases, but there is no reason to believe that this second star formation is linked to a given cosmological time and may not take place at any epoch in the cluster. Figure 16 shows that the blue elliptical can be successfully fitted with the same E+A family models, when the second burst is still ongoing. The galaxy template in Fig. 16 is seen 1.6 Myr after the beginning of the second burst, when the

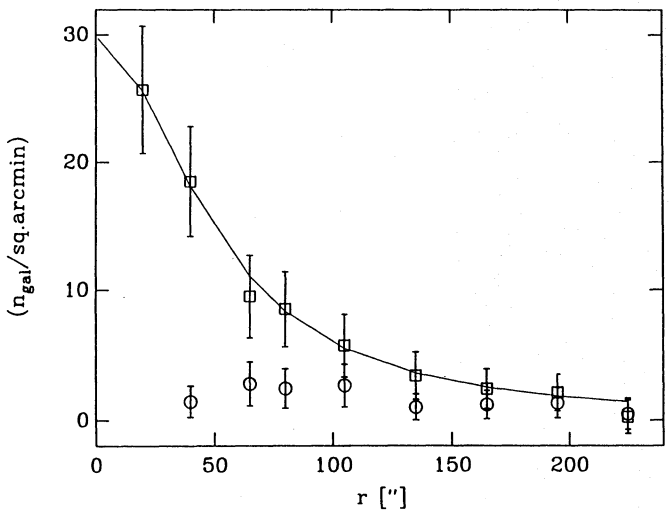

Fig. 15. The projected radial distribution of elliptical and E+A members. The galaxies are sampled up to 90″ radial distance with 20″ step size. Further out the sampling interval is 30″. The distribution of elliptical galaxies is fitted with an analytic King profile, characterized by σ_0=29 galaxies arcmin^{-2} and r_c=50″. The E+As show a much flatter distribution

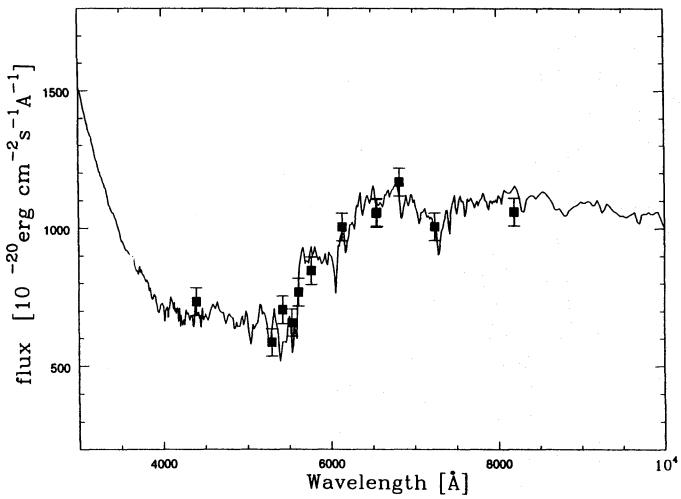

Fig. 16. SED of the galaxy #245 fitted with a E+A model. The galaxy is seen 1.6 Myr after the beginning of the second burst, when the mass in the younger population is only 0.16 % of that in the older galaxy

mass in the younger stellar population is according to (3) only $\Delta M_2 = 0.16\% M_1$.

An analogous case is the galaxy #259 in Fig. 17. The fit of the data points was performed by means of a very young E+A template in which the second burst is still ongoing. At a post-burst age of 0.5 Myr, the mass in the younger population is only 0.05 % of that in the older galaxy (Eq. 3). The SED is basically different from that of a spiral galaxy, because the contribution from the old stars in the underlying E component, makes the continuum above 5000 Å much redder.

Our analysis of E+A galaxies was undertaken under the assumption that their characteristic spectral features can be interpreted as post starburst products. Therefore, in this context the two terminologies are equivalent. This interpretation favors galaxy interactions as the mechanism responsible for triggering recent star formation activity in galaxy clusters. Indeed this is the easiest way we can imagine to rejuvenate the gas content of early-type galaxies and induce star formation. The fact that four out of the six mergers present in Cl0939+472 are E+A galaxies (#189,#208,#259,#365) is a strong hint in this direction. Moreover, the morphology sequence of our E+As correlates fairly well with the sequence of age after the second burst: mergers and irregular galaxies appear to be the youngest post-starburst galaxies (Fig. 11 and Table 8). Interpreted in this context, the E+A galaxies observed could just represent different phases of fading. However, as already pointed out, the merger scenario is not the only explanation.

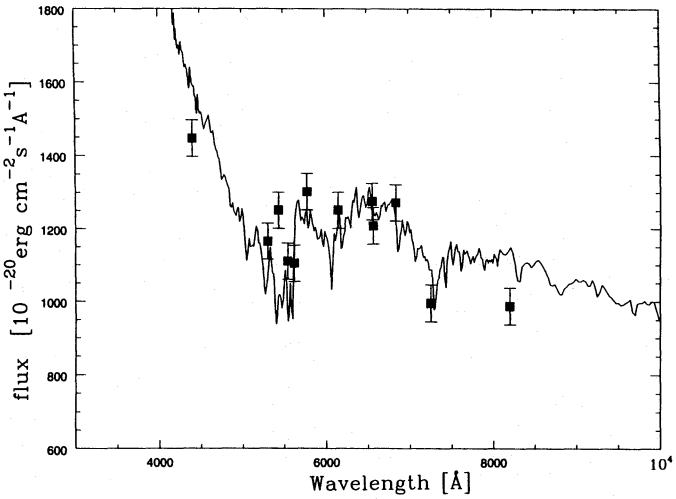

Fig. 17. SED of the galaxy #259 fitted with an E+A model. The galaxy is seen 5 Myr after the beginning of the second burst, when the mass in the younger population is only 0.05 % of that in the older galaxy

The existence of two galaxies (one with a merger morphology) with ongoing bursts confirms that this activity takes place continuously in the cluster. These two cases are certainly a conservative estimate, because no filter was placed on the emission lines that could better detect such ongoing activity. Once again, an analysis of the cluster with a FPI shows its complementary importance in revealing all forms of activity present.

6. Conclusions

In the framework of our long-term project, the study of the galaxy population in medium-high redshift clusters of galaxies, we have analyzed a 5′ × 5′ field in the rich cluster Cl0939+472. We succeeded in obtaining redshifts and morphological classification for 85% of all the objects brighter than R=22.5 mag. By means of E+A templates, we have systematically identified E+A galaxies in this cluster. The templates were computed considering that these galaxies are the result of a strong second episode of star formation in an underlying elliptical or S0 galaxy (post starburst picture). With this procedure we have correctly identi-

fied six already known E+A cluster members and found 29 new ones.

The study of the elliptical population was also undertaken in detail in order to have a reliable estimate of the significance of the E+A phenomenon in the context of the cluster population. Our results confirm, with a large statistical improvement, the high incidence of E+A galaxies in Cl0939+472: (21±7)% of all galaxies classified as member galaxies show signs of an E+A spectrum.

Important information was obtained from HST images that provided the Hubble type for 83 galaxies in our Cl0939+472 field. Of the 35 galaxies that we classify as E+A members, 15 were studied by HST. The six E+A galaxies observed by DG92 are mergers or irregular galaxies. This confirms the importance of mergers/interactions to the E+A phenomenon. However, the majority of E+A galaxies, and in particular all the newly found, look like normal disk-systems, spiral or irregular types. Thus, both mergers/interactions and ram-pressure stripping of galaxies are plausible mechanisms to explain the appearance of E+A galaxies in high redshift clusters. Moreover, the star formation activity in E+A galaxies does not seem to be confined to a particular epoch in the past, but in some galaxies it is currently taking place. In fact, the SEDs of a very blue elliptical galaxy and a merger (Dressler 1993), both confirmed by us as cluster members, can be successfully fitted by E+A models, at the earlier phases of the second burst, when it is still ongoing.

An encouraging result of this work is that the morphological information derived from optimized multifilter photometry, is largely in agreement with that provided by HST imaging observations. This fact points towards the effectiveness of our photometric approach in the recognition of morphological types of distant galaxies and the estimation of their cluster membership.

A systematic analysis of the cluster population characterized by ongoing star formation, realized with a FPI, will be the next observational step to quantify globally this activity in Cl0939+472.

References

Bahcall J.,Soneira R. 1981a, ApJS 47, 357
Bahcall J.,Soneira R. 1981b, ApJ 246, 122
Broadhurst T.J.,Ellis R.S.,Shanks T. 1988, MNRAS, 235, 827
Bruzual A.G. 1983, ApJ 273, 105
Bruzual A.G.,Charlot S. 1993, ApJ 405, 538
Bruzual A.G., Belloni P. 1994, in preparation
Burstein D.,Heiles C 1982, AJ 87, 1165
Butcher H.,Oemler A. 1978, ApJ 219, 18
Butcher H.,Oemler A. 1978, ApJ 226, 559
Butcher H.,Oemler A. 1984, ApJ 285, 426
Buzzoni A. 1989, ApJS 71, 817
Caldwell N.,Rose J.A.,Sharples R.M.,Ellis R.S.,Bower R.G. 1993, AJ 106, 473
Charlot, S., Ferrari, F., Mathews, G.J., & Silk, J. 1993, ApJ, 419, L57
Coleman G.D.,Chi-Chao W., Weedman D.W. 1980, ApJS 43, 393
Colless M.,Ellis R.S.,Taylor K.,Hook R.H. 1990, MNRAS 224, 408
Colless M.,Ellis R.S.,Broadhurst T.J.,Taylor K.,Peterson B.A. 1993, MNRAS 244, 408
Couch W.J.,Ellis R.S.,Godwin J.,Carter D. 1983, MNRAS 205, 1287
Couch W.J.,Sharples R.M. 1987, MNRAS 229, 423
Couch W.J.,Ellis R.,Sharples R,Smail I. 1994, ApJ 430, 121
Cowie L.L.,Songalia A.,Hu E.M. 1992a, Nature 354, 460
Cowie L.L.,Songalia A.,Hu E.M. 1992b, Nature 357, 607
Dressler A.,Gunn J. 1982, ApJ 263, 533
Dressler A.,Gunn J. 1983, ApJ 270, 7
Dressler A.,Thompson I.,Shectman S. 1985, ApJ 288, 481
Dressler A.,Shectman S. 1987, AJ 94, 899
Dressler A. 1992, *STScI Newsletter* 9,2
Dressler A. 1993, ASP , Observational Cosmology, Vol.51, 225, G.Chincarini,A.Iovino,T. Maccacaro and D. Maccagni (eds.)
Dressler A.,Gunn J. 1992, ApJS 78 ,1
Dressler A.,Oemler A.,Butcher H.R.,Gunn J.E.1994, ApJ 430, 107
Ellis R.S.,Couch W.J.,MacLaren I.,Koo D.C. 1985, MNRAS 217, 239
Evrard A.E.,1991,MNRAS 248,8p
González, J.J. 1993, Ph.D. thesis, University of California, Santa Cruz
Gunn J.E.,Oke J.B. 1975, ApJ 195, 255
Gunn J.E.,Stryker L.L. 1983, ApJS 52,121
Kennicutt R.C. 1992 , ApJS 79, 255
Lavery R.,Henry J.P. 1988, ApJ 330, 596
Lavery R.J.,Pierce M.J.,McClure R.D,1992, AJ 104, 2067
Lilly S.J. 1987, MNRAS, 229, 573
Massey P.,Gronwall C. 1990, ApJ 358, 344
Newberry M.,Boroson T.,Kirshner R.,1990, ApJ 350, 585
Pickles A.J., 1985, ApJ 296, 340
Röser H.-J.,Meisenheimer KI. 1991, A&A 252, 458
Thimm G.J.,H.-J.Röser,Hippelein H.,Meisenheimer K. 1994, A&A 285, 785
Small T.A.,Sargent W.L.,Hamilton D. 1993, *Galaxy clusters and large scale structures in the universe*,SISSA,Giuricin G.,Mardirossian F.,Mezzetti M (eds.)
Tyson J.A. 1988, AJ 96,1
Visvanathan S.,Sandage A. 1977, ApJ 216, 214
Worthey, G. 1992, Ph.D. thesis, University of California, Santa Cruz

This article was processed by the author using Springer-Verlag LaTeX A&A style file version 3.